Available online at www.sciencedirect.com
ScienceDirect
Journal of Computational Physics 218 (2006) 398–416
JOURNAL OF COMPUTATIONAL PHYSICS
www.elsevier.com/locate/jcp

Analysis of a new high resolution upwind compact scheme

A.K. De, V. Eswaran *

Department of Mechanical Engineering, Indian Institute Technology Kanpur, Kanpur, Uttar Pradesh 208 016, India

Received 11 August 2005; received in revised form 7 December 2005; accepted 20 February 2006
Available online 19 April 2006

Abstract

A new high-resolution upwind compact scheme is presented and analyzed, along with several previously proposed schemes, for numerical dispersion-dissipation, anisotropy, phase damping, dispersion relation preservation property and numerical stability. The schemes are tested on problems of the propagation of a initially discontinuous wave and of the transport of a sharp scalar cone. A benchmark problem of aeroacoustics is solved with the present scheme, giving satisfactory resolution. The scheme compares well with the existing schemes for the range of properties considered desirable in high resolution schemes.

Keywords: Compact schemes; Dispersion; Dissipation; Stability; DRP; Wave propagation

1. Introduction

Higher-order finite-difference schemes have gained considerable importance in the direct numerical simulation (DNS) of the Navier–Stokes equations as they are generally more robust and less costly than spectral methods [1].

In explicit finite-difference schemes, the derivative at a point is specified explicitly in terms of the function values at that point and its neighbors [2]. Higher-order explicit schemes, however, suffer from cumbersomely large stencil sizes and are not easily amenable to optimization for superior high wavenumber resolution. They also necessitate the use of large one-sided boundary stencils, which often bring in numerical instabilities in the computations. Compact schemes [3–6] are less affected by these problems. Compact schemes couple derivatives and the function values of neighboring points in such a way that a smaller stencil facilitates higher order accuracy as well as superior numerical properties. Of late, upwind compact schemes have received attention as they tend to be less prone to numerical instability and aliasing error than central compact scheme in strongly convective flows.

Upwind schemes, both explicit and compact are developed in several ways. In one, dissipation is artificially added to a central scheme [7–9]. These schemes retain the same stencil as their central counterparts but contain asymmetric coefficients. In another method, an upwind biased asymmetric stencil is chosen with reference to the direction of the flow [10–13]. Apart from this, upwinding by the addition of a spatial filtering term [12],

* Corresponding author. Tel.: +91 512 259 7429; fax: +91 512 259 0007.
E-mail address: eswar@iitk.ac.in (V. Eswaran).

0021-9991/$ - see front matter
doi:10.1016/j.jcp.2006.02.020

using a lower-order scheme in order to optimize it [14], combining first and second order derivatives implicitly in a single equation [15] or using MacCormack-type factorization [16] are some of the other notable approaches for developing upwind compact schemes.

Fourier analysis of numerical schemes (e.g. Refs. [3,10,17]) are a useful way in which a range of their properties can be analyzed. The numerical stability of schemes is an issue of paramount importance. This is usually studied through normal mode analysis, which is referred to as G-K-S stability theory [18,19]. This entails determining the eigen-values of the error evolution matrix which when multiplied by the previous step solution error gives the new time-step solution error. Any scheme with even one eigen-value with a positive real part will be unstable. The advantage of this method is that it takes both boundary and inner schemes into consideration to determine stability.

In compact schemes, optimization can be carried out to enhance the stability of the scheme through the use of parameters left free after a less than-maximum formal order of accuracy is accepted. Zhong [8] used a free parameter to achieve an eigen-value spectrum favorable for the stability of a coupled inner-and-boundary tridiagonal scheme.

In the present work a high resolution upwind compact scheme has been optimized using the degrees of freedom available after adding a 5th order dissipation term to a 6th order scheme It has been shown that spatial filtering added to the central scheme leads to the same upwind scheme. We have also carried out fourier analysis of several explicit and compact schemes with the aim of comparing various properties such as numerical dispersion–dissipation, anisotropic error associated with the numerical phase speed, numerical directional damping, dispersion relation preservation ability and numerical stability in a common framework. The proposed scheme has been tested for problems involving propagation of an initially discontinuous wave and of a sharp gaussian cone and a benchmark problem of aeroacoustics.

In the next section, fourier analysis of finite difference schemes is briefly outlined. In Section 3, the derivation of the present scheme is presented, and it is compared with some earlier proposed schemes in terms of the properties described in Section 2. Section 4 presents results of three numerical tests that are chosen to explore different aspects of the proposed scheme.

2. The new high resolution upwind compact scheme

Compact schemes can be written in a generic form as

$$\sum_{l=-N_1}^{l=N_1} \beta_l f'_{j+l} = \frac{1}{h} \sum_{l=-M_1}^{M_1} a_l f_{j+l}, \quad \beta_0 = 1, \quad \beta_l = \beta_{-l} \tag{1}$$

where the stencil sizes of the implicit and the explicit parts of the scheme are $N = 2N_1 + 1$ and $M = 2M_1 + 1$, respectively. Schemes of different order of accuracy can be derived from the above formula using Taylor series expansion [3]. For instance, with $N_1 = 2$ and $M_1 = 3$ this formula is

$$\beta f'_{j-2} + \alpha f'_{j-1} + f'_j + \alpha f'_{j+1} + \beta f'_{j+2} = \frac{1}{h}(a_{-3}f_{j-3} + a_{-2}f_{j-2} + a_{-1}f_{j-1} + a_0 f_j + a_1 f_{j+1} + a_2 f_{j+2} + a_3 f_{j+3}) \tag{2}$$

A fifth order upwind compact scheme can be formed by adding a 5th order dissipative term to the above formula, i.e.

$$\begin{aligned} &\beta f'_{j-2} + \alpha f'_{j-1} + f'_j + \alpha f'_{j+1} + \beta f'_{j+2} \\ &\quad = \frac{1}{h}(a_{-3}f_{j-3} + a_{-2}f_{j-2} + a_{-1}f_{j-1} + a_0 f_j + a_1 f_{j+1} + a_2 f_{j+2} + a_3 f_{j+3}) + \frac{\gamma}{2n!} h^{2n-1} \left.\frac{\mathrm{d}^{2n} f}{\mathrm{d}x^{2n}}\right|_j \end{aligned} \tag{3}$$

where γ determines the amount of dissipation added.

Upwind compact schemes can also be formed by adding a symmetric filtering term to the asymmetric explicit part of a central compact scheme, i.e.

$$\begin{aligned} \beta f'_{i-2} + \alpha f'_{i-1} + f'_i + \alpha f'_{i+1} + \beta f'_{i+2} = {} & \frac{1}{h}[a_3(f_{i+3} - f_{i-3}) + a_2(f_{i+2} - f_{i-2}) + a_1(f_{i+1} - f_{i-1})] \\ & + \frac{1}{h}[b_3(f_{i+3} + f_{i-3}) + b_2(f_{i+2} + f_{i-2}) + b_1(f_{i+1} + f_{i-1}) + b_0 f_i] \end{aligned} \tag{4}$$

In both the above forms there are nine unknown coefficients. The first seven are obtained by matching terms with the same powers of h, from $O(h^{-1})$ to $O(h^5)$, from both sides of the equation. The remaining two coefficients are obtained from the modified wave number expression whose imaginary part is forced to match the exact one at two different scaled wave numbers, i.e.

$$K_i(\kappa h) = \kappa h, \quad \text{for } \kappa h = 2.5, 2.7$$

These discrete wave numbers are chosen so that the scheme obtained from it gives a near-optimal dispersion property. The coefficients thus obtained from Eq. (3) are

$$\begin{aligned} &a_{\pm 3} = \pm 0.00559 + 0.0014\gamma, \quad a_{\pm 2} = \pm 0.25154 - 0.0083\gamma, \quad a_{\pm 1} = \pm 0.6494 + 0.0208\gamma, \\ &a_0 = -0.0278\gamma, \quad \alpha = 0.57967, \quad \beta = 0.0895 \end{aligned} \tag{5}$$

The same coefficients result from Eq. (4) as from (5) with γ chosen -1. This shows that the addition of a symmetric filtering term is equivalent to adding a dissipation term. The value of $\gamma = -1$ is chosen for all the results presented below.

2.1. Other schemes

The new upwind compact scheme, from now on termed the "N" scheme, will now be compared with the previously proposed compact and explicit schemes mentioned below:

(1) *Spectral like central compact scheme* (SLS)
This scheme was proposed by Lele [3]. This is a 6th order pentadiagonal scheme given by

$$\begin{aligned} &0.0895(f'_{i-2} + f'_{i+2}) + 0.57967(f'_{i-1} + f'_{i+1}) + f'_i \\ &\quad = \frac{1}{h}[0.00559(f_{i+3} - f_{i-3}) + 0.25154(f_{i+2} - f_{i-2}) + 0.6494(f_{i+1} - f_{i-1})] \end{aligned}$$

(2) *Optimized upwind compact scheme* (Z)
This is a 5th order tridiagonal scheme proposed by Zhong [8]:

$$25f'_{j-1} + 60f'_j + 15f'_{j+1} = \frac{1}{h}\left(-\frac{5}{2}f_{j-2} - \frac{160}{3}f_{j-1} + 15f_j + 40f_{j+1} + \frac{5}{6}f_{j+2}\right)$$

(3) *Wave number extended explicit scheme* (L)
This is a 4th order wavenumber extended upwind biased scheme proposed by Li [10]:

$$f'_i = \frac{1}{h}(-0.055453f_{i-3} + 0.3606f_{i-2} - 1.221201f_{i-1} + 0.554534f_i + 0.3894f_{i+1} - 0.2788f_{i+2})$$

(4) *Tam and Webb's DRP scheme* (TW)
Tam and Webb [20] formulated a 4th order explicit scheme with enhanced spectral resolution:

$$f'_i = \frac{1}{h}[0.02651995(f_{i+3} - f_{i-3}) - 0.18941314(f_{i+2} - f_{i-2}) + 0.79926643(f_{i+1} - f_{i-1})]$$

(5) *A fifth order upwind explicit scheme*
This scheme is formed by adding a 5th order dissipation term with a 6th order central scheme and optimizing the diffusion coefficient from the eigenvalue spectrum obtained in the stability analysis.

$$f'_i = \frac{1}{h}\left(-\frac{1}{40}f_{i-3} + \frac{19}{120}f_{i-2} - \frac{7}{8}f_{i-1} + \frac{1}{6}f_i + \frac{5}{8}f_{i+1} - \frac{1}{10}f_{i+2} + \frac{1}{120}f_{i+3}\right)$$

3. Fourier analysis of finite difference schemes

All the analyses presented here are based on the first order wave equation, given by

$$u_t + cu' = 0 \tag{6}$$

3.1. Numerical dispersion and dissipation

A solution $u(x,t)$ is represented by a typical fourier mode, i.e.

$$u = \hat{u}_\kappa(t)\mathrm{e}^{\mathrm{i}\kappa x} \tag{7}$$

where $\hat{u}_\kappa$ is the Fourier mode of wave number κ, and $\mathrm{i} \equiv \sqrt{-1}$. After exact spatial differentiation

$$u' = \mathrm{i}(\kappa h)\frac{\hat{u}_\kappa}{h}\mathrm{e}^{\mathrm{i}\kappa x} \tag{8}$$

where the wavenumber is scaled by the grid interval $h = L/N$, where L is the length of the domain and N is the number of grid intervals. By analogy, the numerical approximation of the derivative can be written as

$$u' = K_{\mathrm{eq}}(\kappa h)\frac{\hat{u}_\kappa}{h}\mathrm{e}^{\mathrm{i}\kappa x} = (K_{\mathrm{r}}(\kappa h) + \mathrm{i}K_{\mathrm{i}}(\kappa h))\frac{\hat{u}_\kappa}{h}\mathrm{e}^{\mathrm{i}\kappa x} \tag{9}$$

where the equivalent wavenumber, $K_{\mathrm{eq}}(\kappa h)$, has real and imaginary parts K_{r} and K_{i} respectively. It can easily be shown that the real part of $K_{\mathrm{eq}}(\kappa h)$ tends to amplify/attenuate the corresponding fourier mode while the imaginary part introduces a phase error. Thus the deviations of the real and imaginary parts of $K_{\mathrm{eq}}(\kappa h)$ from the exact scaled wavenumber can be respectively taken to be the indicators of numerical dissipation and dispersion.

Fig. 1 shows the imaginary part of the modified wavenumber $K_{\mathrm{i}}(\kappa h)$ for the schemes discussed above. The straight line marked g is the exact value, while the other curves depict the $K_{\mathrm{eq,i}}$ of the various schemes. Clearly the compact schemes are superior compared to the explicit schemes as they match the exact value over a greater range of wave numbers. It can be shown that the SLS and the N schemes have the same dispersion property if $\gamma = 0$. Fig. 1 shows that even with $\gamma = -1$ the dispersion is almost identical in the two schemes. The Z scheme lies between these two schemes and the explicit schemes. The explicit schemes have somewhat poorer resolution although they are still significantly better than the conventional 2nd(CDS2) and 4th(CDS4) order central difference scheme which are also shown. The L scheme and the TW schemes have nearly the same dispersion property.

In Fig. 2, the real part of the modified wavenumber which is the indicator of numerical dissipation is plotted for different schemes. The center-difference schemes have no dissipation and are not shown. Fig. 2 shows that, of the two upwind compact schemes, the N scheme has much higher dissipation in the high wavenumber range compared to the Z scheme, while dissipation is almost the same at lower wavenumbers. The two explicit schemes have higher dissipation at lower wave numbers compared to the compact schemes, with the L scheme having considerably higher dissipation compared to the 5U scheme. The N scheme has arguably the best

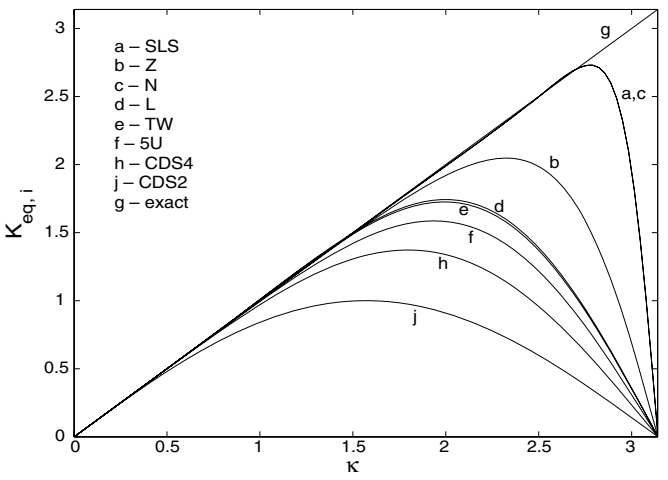

Fig. 1. Numerical dispersion of the schemes.

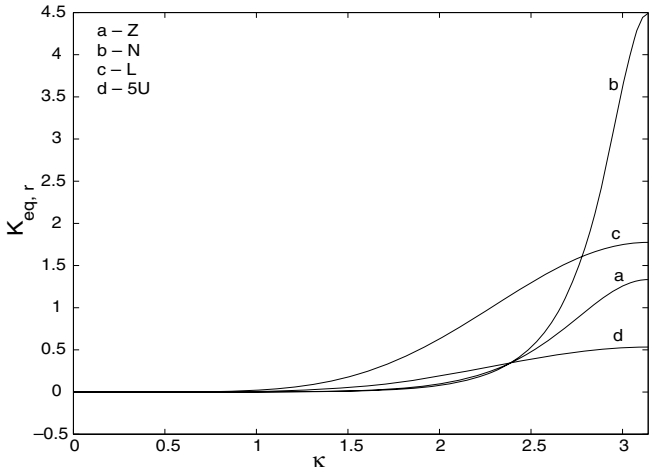

Fig. 2. Numerical dissipation of the upwind schemes.

dissipation profile of the dissipative schemes – it has high dissipation at very high wavenumbers, enhancing numerical stability and reducing aliasing errors, while having low dissipation at lower wavenumbers, enhancing accuracy.

3.2. Phase speed anisotropy and directional damping

If Eq. (9) is substituted into Eq. (6), we get

$$\frac{1}{\hat{u}_\kappa}\frac{\mathrm{d}\hat{u}_\kappa}{\mathrm{d}t} = -\frac{c^*}{h}\mathrm{i}\kappa h \tag{10}$$

where $c^* = c\frac{K_\mathrm{r}(\kappa h)+\mathrm{i}K_\mathrm{i}(\kappa h)}{\mathrm{i}\kappa h}$, is the numerical wave speed at which the approximate solution travels, in comparison to the exact wave speed c.

In 2-D flows, if a wave propagates at an angle θ to the x-axis then the spectral representation of its typical fourier mode is

$$u = \hat{u}_\kappa \mathrm{e}^{\mathrm{i}\kappa s} \quad \text{where } s = x\cos\theta + y\sin\theta \tag{11}$$

and the numerical phase speed becomes

$$\frac{c^*}{c} = \frac{K_\mathrm{eq}(\kappa h\cos\theta)\cos\theta + K_\mathrm{eq}(\kappa h\sin\theta)\sin\theta}{\mathrm{i}(\kappa h)} \tag{12}$$

with a real part

$$\Re\left(\frac{c^*}{c}\right) = \frac{K_\mathrm{i}(\kappa h\cos\theta)\cos\theta + K_\mathrm{i}(\kappa h\sin\theta)\sin\theta}{\kappa h} \tag{13}$$

and imaginary part

$$\Im\left(\frac{c^*}{c}\right) = -\frac{K_\mathrm{r}(\kappa h\cos\theta)\cos\theta + K_\mathrm{r}(\kappa h\sin\theta)\sin\theta}{\kappa h} \tag{14}$$

The extent to which the real part of the numerical wave speed $\Re(\frac{c^*}{c})$ varies with θ is a measure of phase speed anisotropy, while the imaginary part gives the measure of numerical damping, because the real part of the modified wavenumber, responsible for the numerical dissipation, is equal to $-\kappa h\Im(\frac{c^*}{c})$.

Fig. 3 shows $\Re(\frac{c^*}{c})$ obtained for the various schemes being studied in polar diagrams. The radial distance of the curves from the origin corresponds to the magnitude of $\Re(\frac{c^*}{c})$ for that angle. The plots are drawn for five different wave numbers $(\frac{6\pi}{10}, \frac{7\pi}{10}, \ldots, \pi)$. At any wavenumber, the exact dispersion property lies on the circle, i.e.

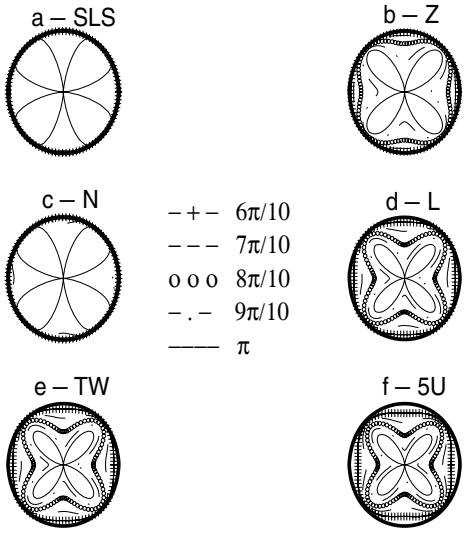

Fig. 3. Phase speed anisotropy of the schemes.

$\frac{c^*}{c} = 1$. Also, any deviation from a circular form indicates anisotropy for that wavenumber. The plots show that for the compact schemes anisotropic error only occurs at highest two wave numbers while the explicit schemes suffer at almost all depicted wave numbers. The SLS and N schemes show similar anisotropic error, at only the highest wavenumber, while the Z scheme has error even at lower wave numbers. The N scheme therefore compares with the best of the other schemes on having the least anisotropy in dispersion.

The expression $K_r(\kappa h\cos\theta)\cos\theta + K_r(\kappa h\sin\theta)\sin\theta$ gives a measure of the variation of numerical dissipation with direction θ. In the polar plots of Fig. 4, this quantity is shown in the radial direction versus θ. The plots are drawn for six different wave numbers $(\frac{\pi}{6}, \frac{\pi}{3}, \ldots, \pi)$. The N scheme is similar to the Z scheme with both showing little anisotropy for $\kappa \leqslant 2\pi/3$. However, as dissipation is quite low in both schemes for $\kappa \leqslant 5\pi/6$ (see Fig. 4), anisotropy in the dissipation will have little effect in that range. Among the explicit schemes, 5U scheme has relatively higher dissipation at all wave numbers, but shows the least anisotropy. For all

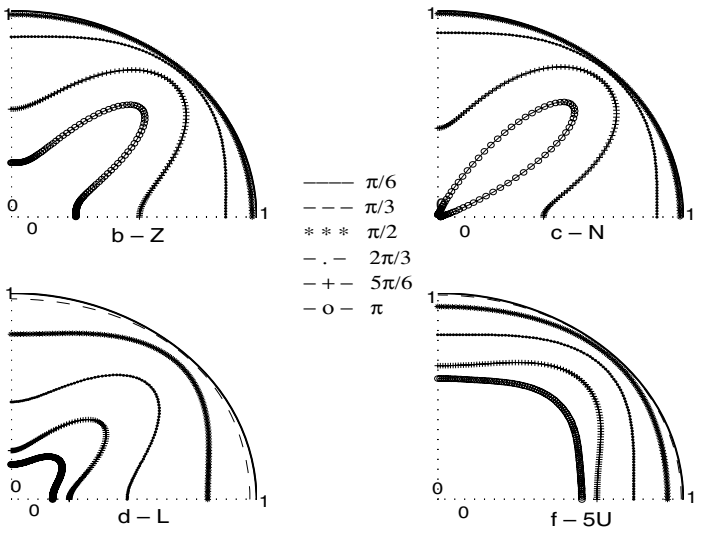

Fig. 4. Directional numerical damping of the upwind schemes.

the schemes, the dissipation is maximum when the direction of flow makes an angle $\frac{\pi}{4}$ with the coordinate direction.

3.3. Dispersion relation preservation (DRP) property

A numerical solution of convective problem must also accurately capture the relationship between the frequency (ω) and the wavenumber (κ) of fourier modes. For the exact solution of equation (6)

$$\frac{\mathrm{d}\omega}{\mathrm{d}\kappa} = c \tag{15}$$

where ω is the frequency of the mode. If the mode $\hat{u}(\omega,\kappa)\mathrm{e}^{\mathrm{i}}(\kappa x - \omega t)$ is inserted into the discretized equation, the numerical group velocity can also be obtained. Taking the time integration scheme to be Euler explicit, the discretized form of the wave equation (6) we get

$$\frac{\mathrm{d}\omega}{\mathrm{d}\kappa}|_{\text{numerical}} = -\mathrm{i}c\mathrm{e}^{\mathrm{i}\omega\Delta t}\frac{\mathrm{d}K_{\text{eq}}(\kappa h)}{\mathrm{d}(\kappa h)} \tag{16}$$

as opposed to the exact expression obtained in Eq. (15). The real part of $\frac{\mathrm{d}\omega}{\mathrm{d}\kappa}|_{\text{numerical}}$ given by

$$\Re\left(\frac{\mathrm{d}\omega}{\mathrm{d}\kappa}|_{\text{numerical}}\right) = c\left(\sin(\omega\Delta t)\frac{\mathrm{d}K_{\mathrm{r}}(\kappa h)}{\mathrm{d}(\kappa h)} + \cos(\omega\Delta t)\frac{\mathrm{d}K_{\mathrm{i}}(\kappa h)}{\mathrm{d}(\kappa h)}\right) \tag{17}$$

characterizes the dispersion relation preservation (DRP) property of the scheme and shows how the simulated waves of various frequency-wavenumber combinations travel in the numerical solution. A superior numerical technique will have a DRP relation which is close to the exact one, Eq. (15), over a large region in ($\omega\Delta t - \kappa h$) plane.

The DRP property of the various schemes being studied is shown Fig. 5. The region where $\frac{1}{c}\Re(\frac{\partial\omega}{\partial\kappa}|_{\text{numerical}})$ lies between 0.95 and 1 is shaded. Thus, in the shaded region, the dispersion relation is preserved to within 5% of the exact value. The N scheme shows the best DRP property for the three compact schemes, as it has the largest contiguously shaded area. The L scheme seems best among the explicit schemes. All the schemes are

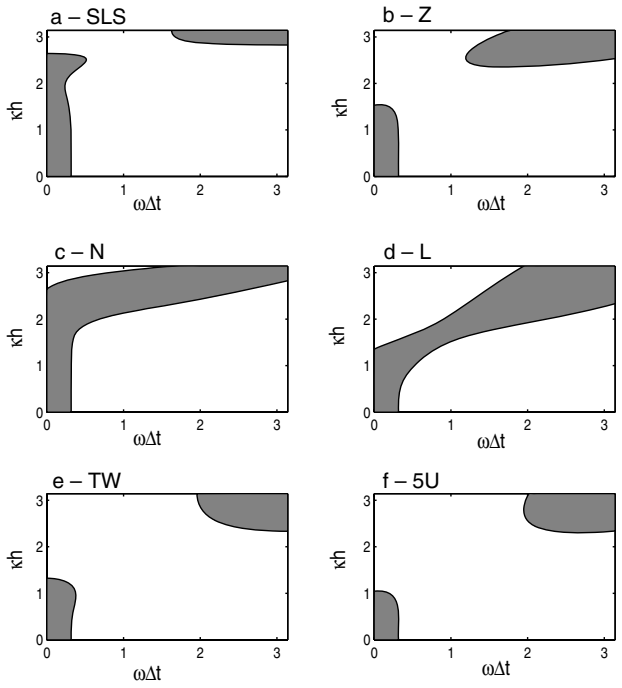

Fig. 5. DRP region for the schemes.

DRP compliant primarily in the low $\omega\,\Delta t$-low κh and high $\omega\Delta t$-high κh region. With the addition of dissipation, the intermediate region become more DRP compliant for both compact and explicit schemes.

3.4. Stability analysis by the matrix method

In GKS stability theory the error is modeled as a Fourier mode:

$$\overline{u} = \hat{u}e^{\lambda t} \tag{18}$$

where $\overline{u}$ is the error associated with the solution of equation 6. For any spatial discretization technique including both inner and boundary schemes the spatial derivative $\overline{u'}$ of $\overline{u}$ can be written in the following matrix form

$$A\overline{u'} = B\overline{u} \tag{19}$$

where $\overline{u'}, \overline{u}$ are respectively the vectors containing the nodal values and A, B are respectively the matrices of the implicit and the explicit parts of the scheme. Substituting $\overline{u} = \hat{u}e^{\lambda t}$ and $\overline{u'} = A^{-1}B\overline{u}$ into the wave equation (6), the following eigen value problem is obtained

$$\left(E - \frac{\lambda}{c}I\right)\hat{u} = 0 \tag{20}$$

where $\frac{\lambda}{c}$ are the eigenvalues of $E \equiv -A^{-1}B$. As positive real parts of λ mean that the error will grow (c.f Eq. (18)) exponentially, for a scheme to be stable, the eigenvalue spectrum of the matrix E should lie left to the $\lambda_r = 0$ line in the $(\lambda_r - \lambda_i)$ plane. That is

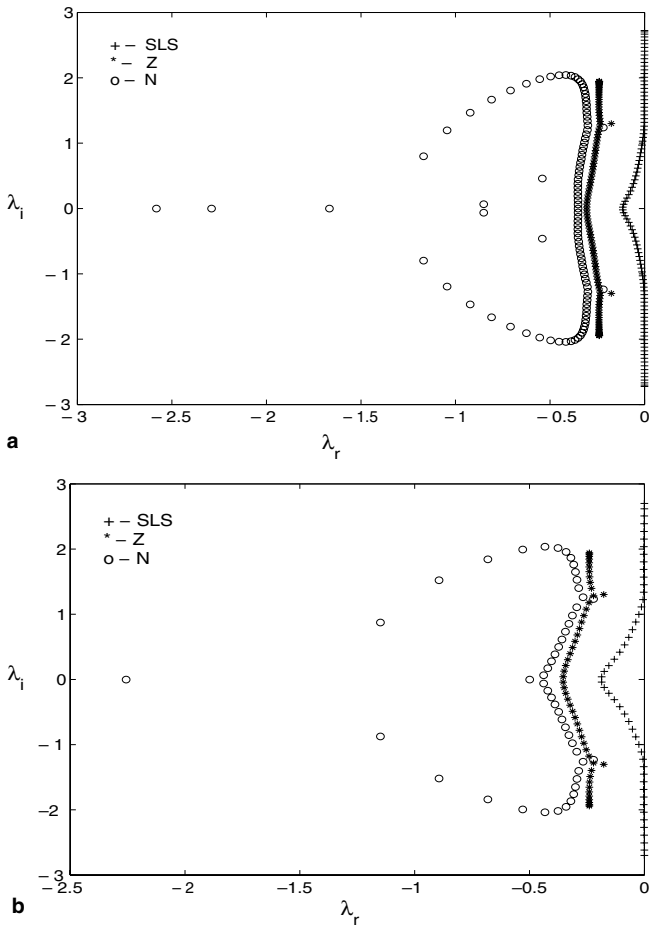

Fig. 6. Eigen value spectrum for the compact schemes, (a) $n = 100$, (b) $n = 50$.

$$\max(\Re(\lambda_i)) < 0, \quad i = 1, \ldots, n \tag{21}$$

for a domain with n grid points.

Figs. 6 and 7 show the eigenvalues arising from the stability analysis of the various schemes. Fig. 6 shows the eigen-values of the three compact schemes for a size of the matrix E (see Eq. (20)) of $n = 100$ and 50, respectively in Fig. 6(a) and (b). All the eigenvalues lie in the left half-plane in the $\lambda_r - \lambda_i$ plane, showing the schemes are stable. The N scheme has the best stability property, with its spectrum showing the most negative values of λ_r. Numerical tests show that $\gamma = -1$ gives the most favorable eigenvalue spectrum for the N scheme. Fig. 7(a) and (b) show the spectra for the explicit schemes for $n = 100$ and 50, respectively. The TW scheme, being a central scheme, has its spectrum nearest to the $\lambda_r = 0$ line, while L scheme gives the best spectrum from the viewpoint of numerical stability.

To summarize, the N scheme compares well with existing compact schemes in terms of numerical stability, dispersion, anisotropy, DRP properties and introduces dissipation at (only) the highest wavenumbers, enhancing stability and reducing aliasing and spurious oscillations (see below).

4. Numerical experiments

Three numerical tests were carried out to evaluate the performance of the schemes in the light of the properties discussed above. It is difficult to judge all the properties of a scheme with a single test, so each test emphasizes different aspects of the schemes.

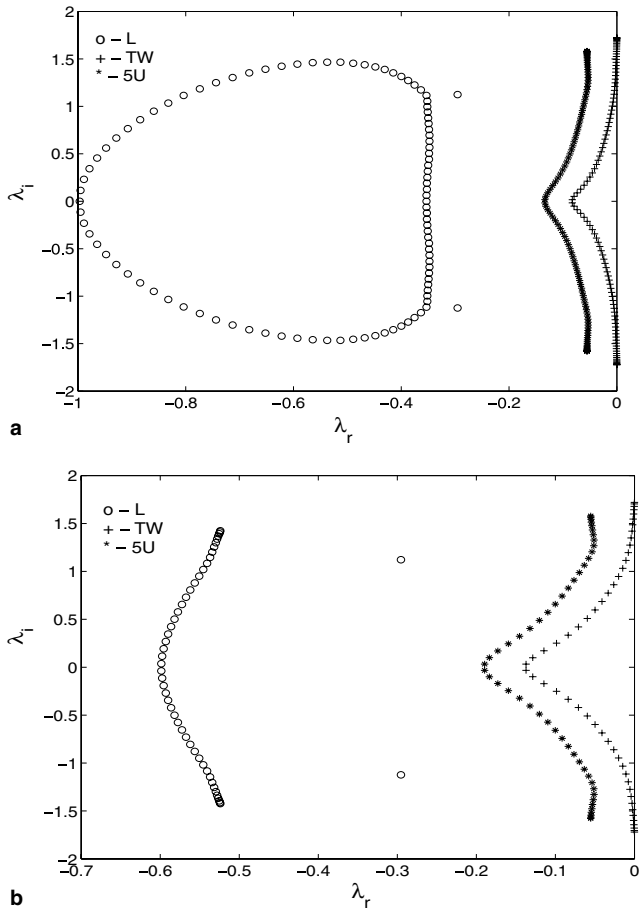

Fig. 7. Eigen value spectrum for the explicit schemes, (a) $n = 100$, (b) $n = 50$.

4.1. Linear wave propagation

In this problem [9] the first order linear 1-D wave equation with wave speed $c = 0.05$ is solved in the $0 \leqslant x \leqslant 1$ domain with $n = 100$ grid points.

$$\frac{\partial u}{\partial t} + c\frac{\partial u}{\partial x} = 0$$

with a boundary condition $u = 0$ at $x = 0$. A cosine profile of periodicity $\frac{1}{5}$ and amplitude 0.5 is the given initial condition

$$u(x, t = 0) = 0.5\cos(10\pi x) \quad 0 \leqslant x \leqslant 1$$

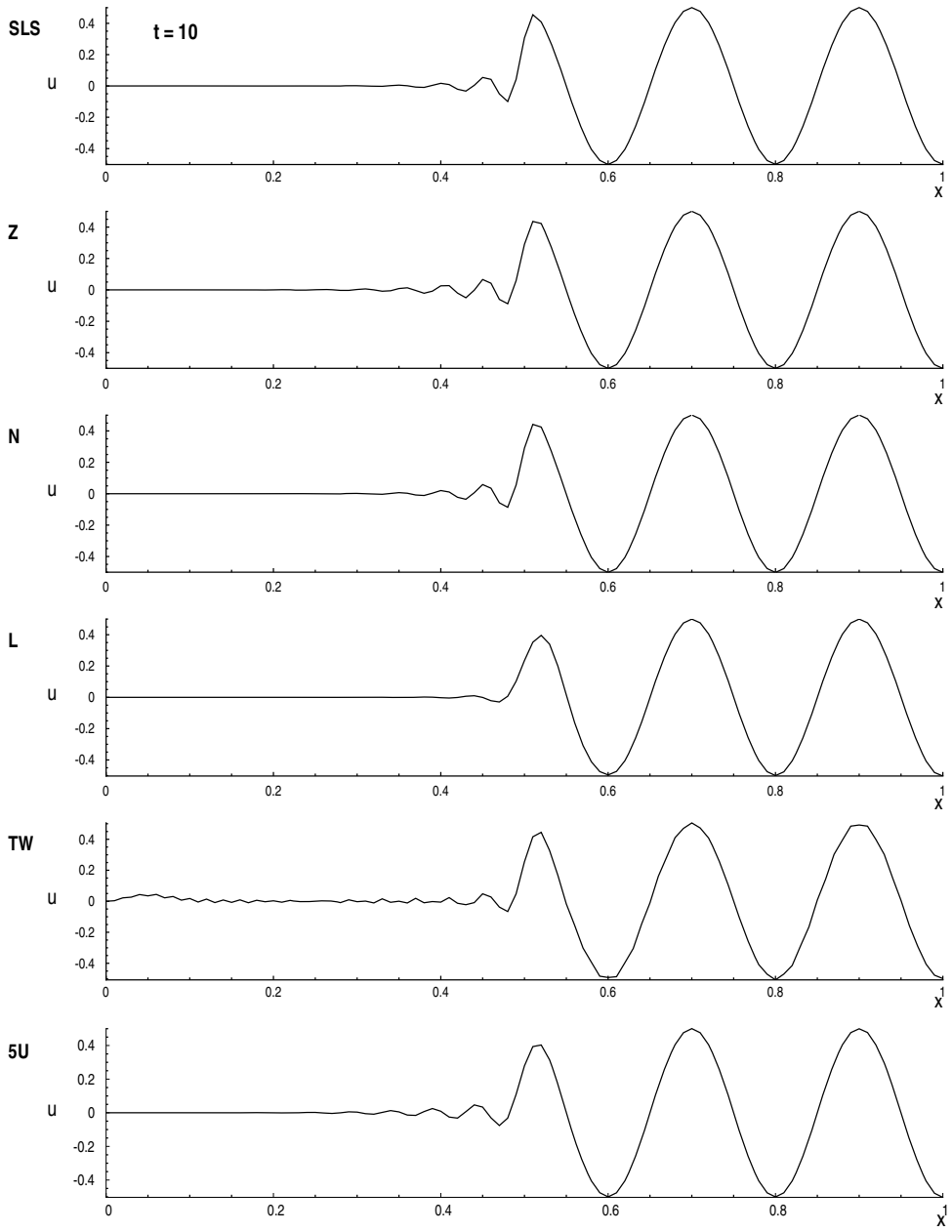

Fig. 8. Profile of the wave at $t = 10$.

The solution has a discontinuity which starts at $x = 0$ and, at $t = 20$, passes through the domain. A long time integration has been performed to see the stability property of the schemes. Euler explicit time integration with $\Delta t = 10^{-4}$ is used to time march the discretized equations. The Courant number for this calculation is $C = \frac{c\Delta t}{h} = 5 \times 10^{-4}$. The results are shown in Figs. 8–12 for $t = 10$, 25, 30, 60 and 100 respectively. Note that Figs. 9–12 have differing scales, adjusted to the degree of spurious oscillations produced in each scheme after the solution has passed through the domain. The results show that SLS and TW solutions leave numerical oscillations in the domain long after the wave passes through it. This is because, being central schemes, they have no dissipation to damp out the spurious oscillations caused by the discontinuity. The compact upwind schemes having dissipation suppress these oscillations. Among these, the N scheme is somewhat better than the Z scheme as can be seen from the results at $t = 25$, 30. There are no oscillations with either scheme after

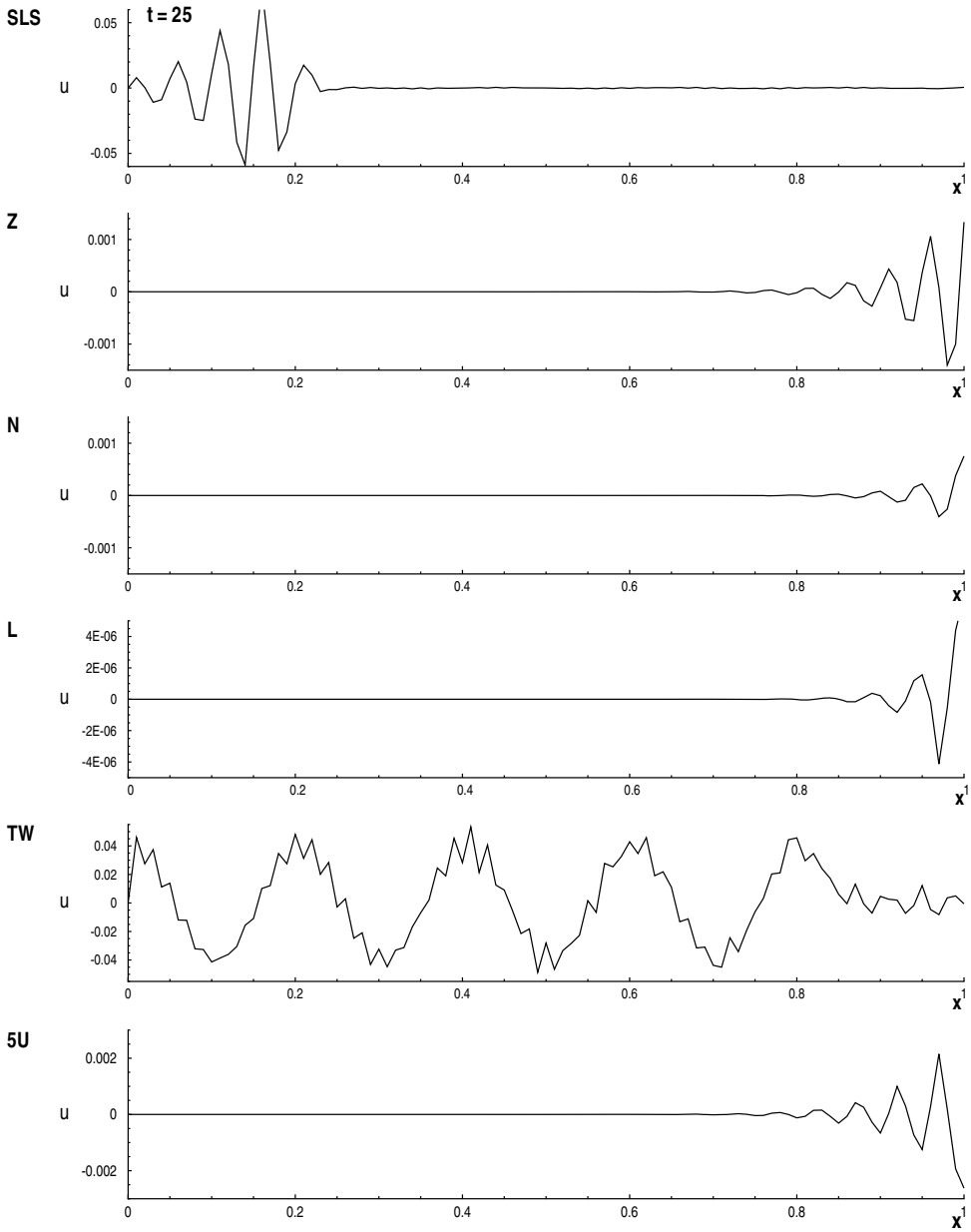

Fig. 9. Profile of the wave at $t = 25$.

$t = 30$. Among the explicit schemes, the L scheme has the best stability property among all schemes compact and explicit as seen from this test; the 5U scheme which has some dissipation, while the TW scheme suffers significantly from spurious oscillations. The N scheme seems the best of the compact schemes considered, and is overall second only to the explicit schemes.

4.2. Rotation of a sharp scalar cone

In this test, a sharp 2-D Gaussian profile is convected along a circle in a unit square domain. The convection-diffusion equation for a scalar ϕ given by

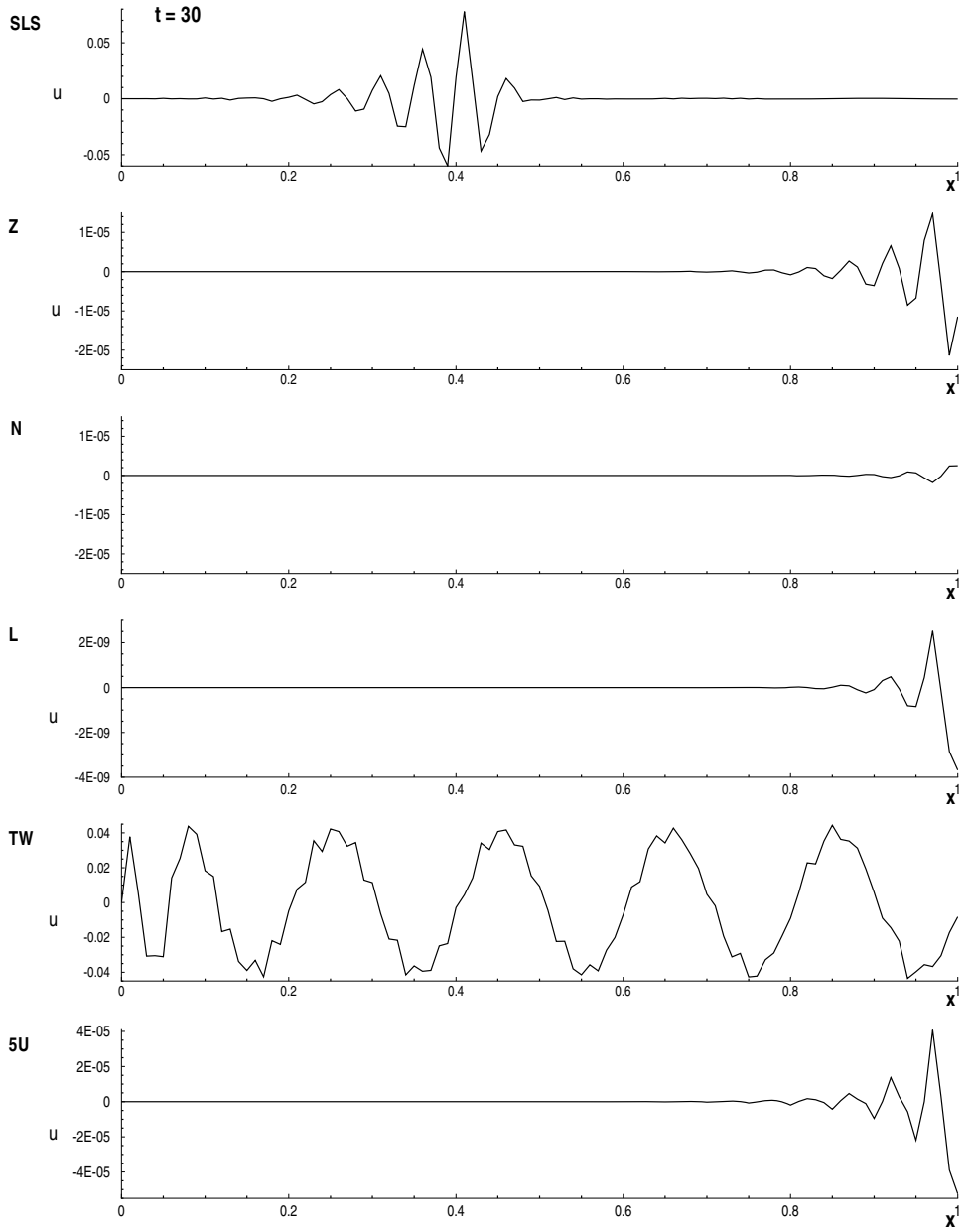

Fig. 10. Profile of the wave at $t = 30$.

$$\frac{\partial \phi}{\partial t} + u\frac{\partial \phi}{\partial x} + v\frac{\partial \phi}{\partial y} = \alpha\left(\frac{\partial^2 \phi}{\partial x^2} + \frac{\partial^2 \phi}{\partial y^2}\right)$$

is solved in the domain $-0.5 \leqslant x \leqslant 0.5$, $-0.5 \leqslant y \leqslant 0.5$ with 65×65 grid points. A sharp Gaussian profile is given as the initial condition as

$$\phi(x, y, t = 0) = a \exp[-\omega[(x - x_c)^2 + (y - y_c)^2]]$$

with $a = 5$, $\omega = 1500$, $x_c = -0.25$, $y_c = 0$ which gives a peak value of 5. The velocity components, taken as $u = -y$ and $v = x$, are such that the initial scalar field rotates about the origin. The diffusive term in the transport equation is switched off ($\alpha = 0$), so the initial profile should be convected undistorted around the origin. A 4th order Runge–Kutta time integration method is used with $\Delta t = 1 \times 10^{-3}$ and results are shown at $t = 2\pi$

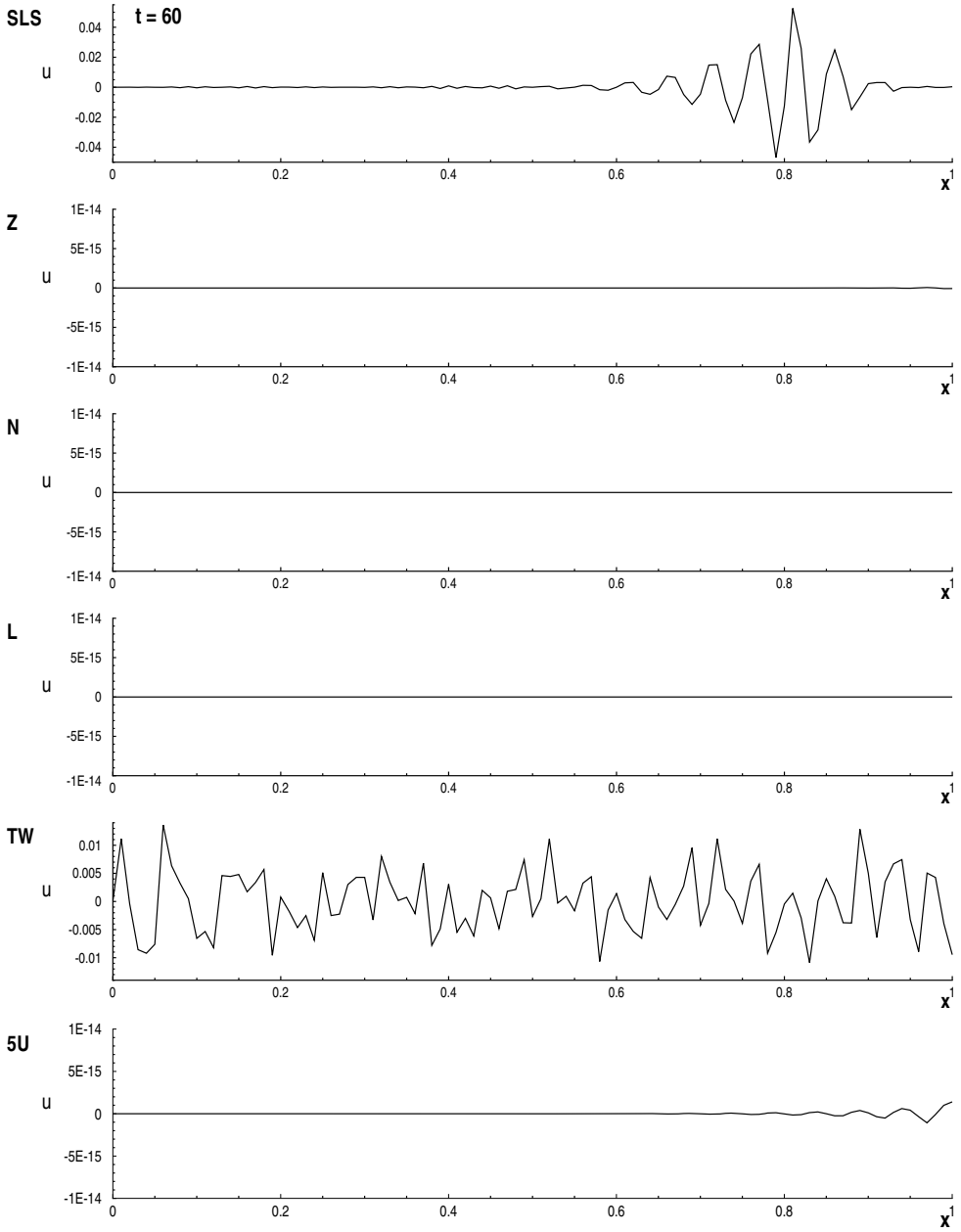

Fig. 11. Profile of the wave at $t = 60$.

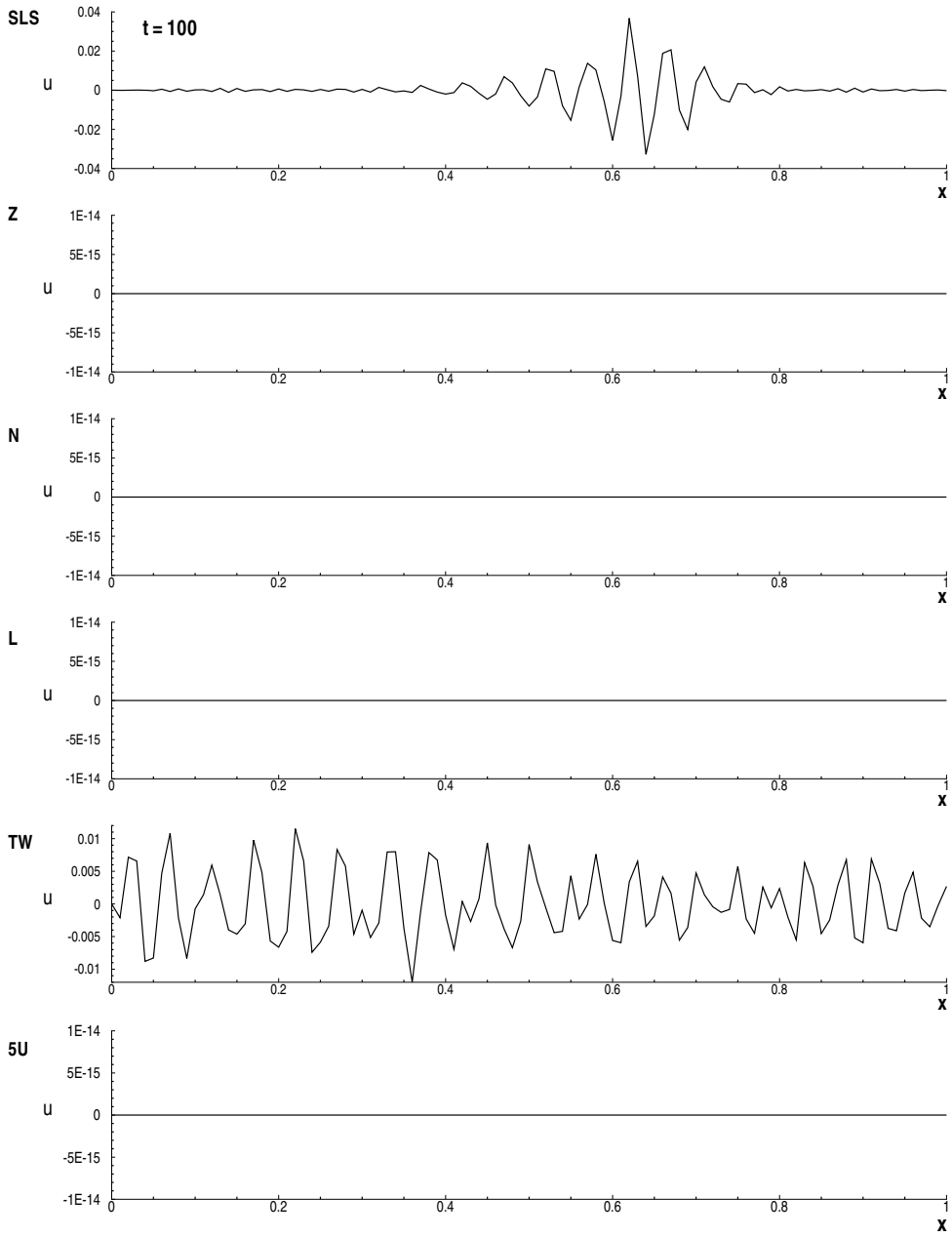

Fig. 12. Profile of the wave at $t = 100$.

when the initial profile completes a full rotation. As the initial profile has high wavenumber components this test evaluates both the spectral resolution as well as the dissipation associated with the spatial discretization scheme. At $t = 2\pi$, the minimum value of $\phi(x, y)$, compared with its initial zero value, is a measure of the numerical oscillation caused by the schemes, and the maximum value of $\phi(x,y)$, reduced from its initial value of 5, indicates the effect of dissipation of the schemes.

Figs. 13 and 14 respectively show the scalar field computed by the compact and explicit schemes, at $t = 2\pi$. Fig. 13 shows that SLS scheme has the best resolution while N scheme is second-best. The N scheme has less oscillation and dissipation compared to the Z scheme. Thus, although the N scheme has the same dispersion property as that of the SLS scheme, it cannot resolve the cone as well as the SLS scheme owing to the dissipation it has at large wavenumbers. Fig. 14 shows the results for the three explicit schemes. Clearly the

explicit schemes are inferior and have high numerical dissipation. The TW scheme suffers from numerical oscillations, but is best in resolving the peak, nearly as well as the compact Z scheme. The L and the 5U schemes, suppress oscillations but are poorer in resolving the peak.

4.3. Linear acoustics

Small amplitude disturbances superimposed on a uniform mean flow of density ρ_0, pressure p_0 and velocity u_0 in the x direction can be described by the two-dimensional linearized Euler equations. These equations are non-dimensionalized as given in [20]:

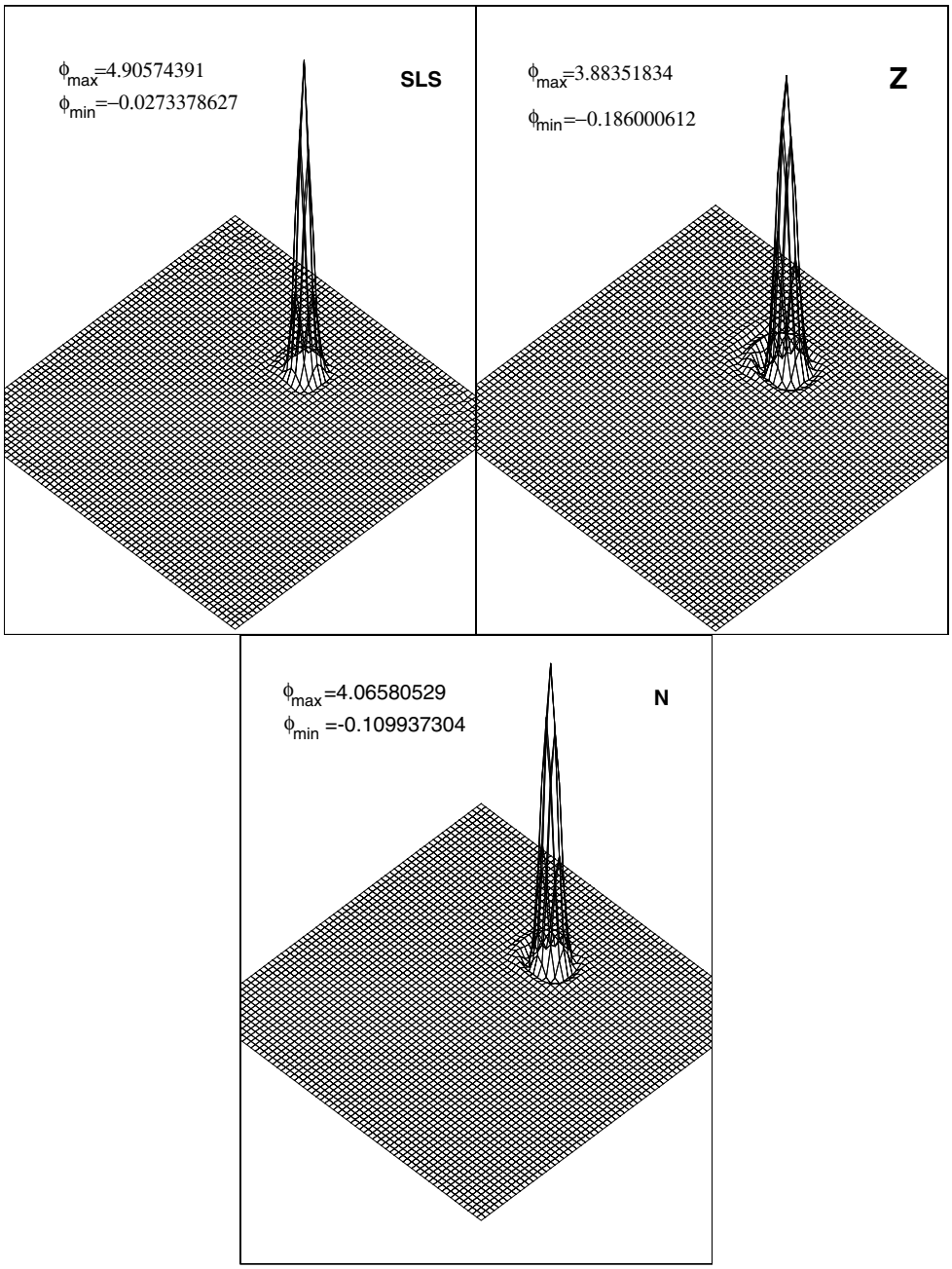

Fig. 13. The sharp cone after a complete rotation for the compact schemes.

$$\frac{\partial \mathbf{V}}{\partial \tau} + \frac{\partial \mathbf{H}}{\partial x} + \frac{\partial \mathbf{J}}{\partial y} = 0 \tag{22}$$

where

$$\mathbf{V} = \begin{bmatrix} \rho \\ u \\ v \\ p \end{bmatrix}, \quad \mathbf{H} = \begin{bmatrix} u + M\rho \\ Mu + p \\ Mv \\ Mp + u \end{bmatrix}, \quad \mathbf{J} = \begin{bmatrix} v \\ 0 \\ p \\ v \end{bmatrix}$$

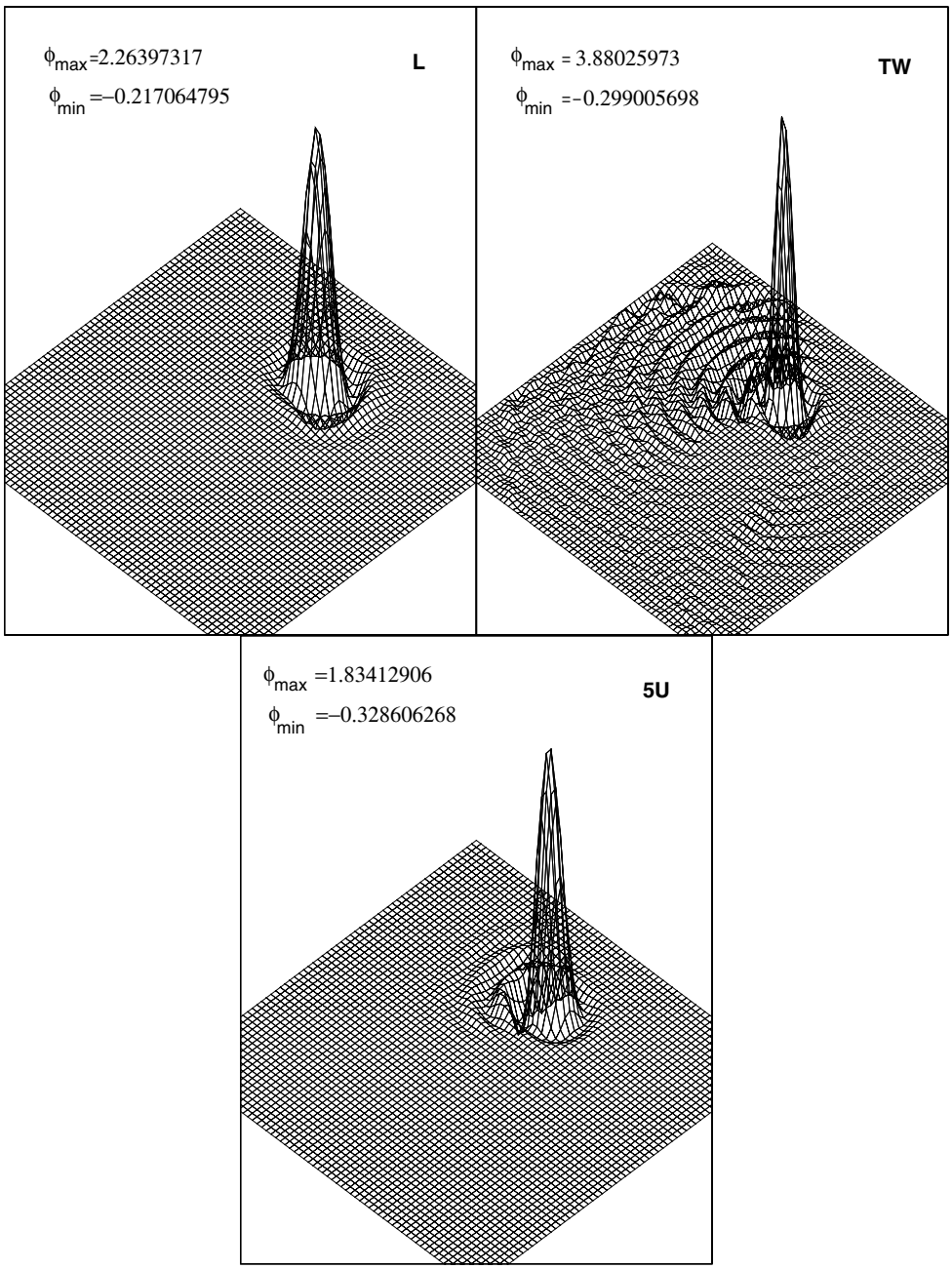

Fig. 14. The sharp cone after a complete rotation for the explicit schemes.

and $M = \frac{u_0}{a_0}$ is the free stream Mach number. The radiation and outflow boundary and initial conditions of Tam and Webb [20] are used in this simulation.

The DRP time integration scheme of Tam and Webb [20] has been used in the present work to time-step the governing Eqs. (22). This is a four level scheme given by

$$\mathbf{U}^{n+1} \simeq \mathbf{U}^n + \Delta t \sum_{i=0}^{3} a_i \left(\frac{\mathrm{d}\mathbf{U}}{\mathrm{d}t}\right)^{n-i}$$

where $a_0 = 2.30255809$, $a_1 = -2.49100760$, $a_2 = 1.57434093$, $a_3 = -0.38589142$. The SLS and N schemes are used as the inner scheme while a second order one-sided difference scheme [9] given by

$$f'_1 = \frac{1}{2\Delta x}(-3f'_1 + 4f'_2 - f'_3) \quad \text{and} \quad f'_N = \frac{1}{2\Delta x}(3f'_N - 4f'_{N-1} + f'_{N-2})$$

is used at the boundaries for better stability. A free-stream Mach number $M = 0.5$, and $\Delta t = 0.05$ with 201×201 grids are used in all the computations. Exact solutions given in [20] are used for comparison.

Fig. 15 shows the pressure waveform along the x axis at $t = 30$ and $t = 65$ respectively for the SLS and N schemes. Both the schemes give a close match with the exact solution. The N scheme, being dissipative in nature, falls slightly short of the sharp peak near the exit boundary (see Fig. 15(b)). Otherwise, there is no

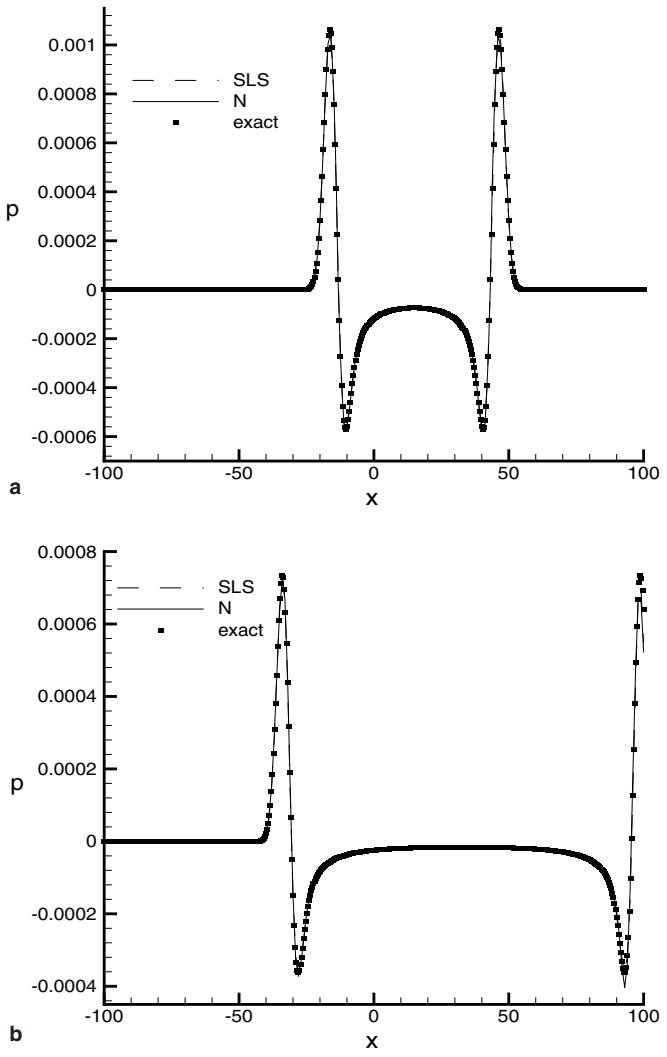

Fig. 15. Pressure waveform along x axis, $y = 0$, at (a) $t = 30$ and (b) $t = 65$ for the compact schemes.

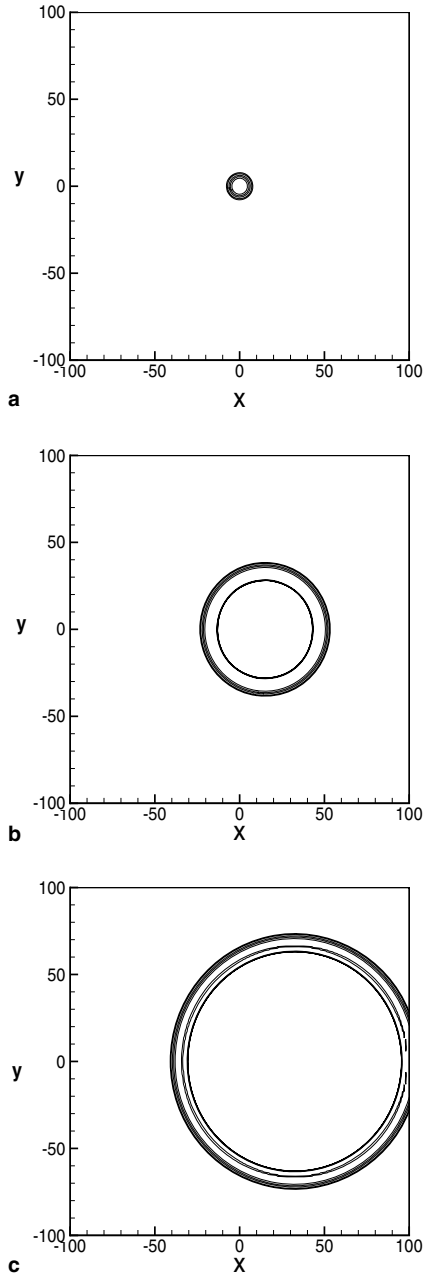

Fig. 16. Pressure disturbance contours at (a) $t = 0$, (b) $t = 30$ and (c) $t = 65$, contours are shown for the maximum amplitude and 20%, 10%, 5%, 2% and 1% levels of it.

discernible difference between the solutions of the two schemes. Thus the N scheme has very nearly the same resolution property as the SLS scheme. Fig. 16 shows the spreading of the pressure disturbance from the initial Gaussian waveform at two different times, as obtained with the N scheme. It is clear from the figure that no numerical oscillation appears even for long time integration.

5. Conclusions

A high resolution and stable pentadiagonal upwind compact scheme is proposed. Numerical dispersion constraints as well as asymptotic stability analysis is used to optimize the scheme. Comparison with previously

proposed schemes show that the present scheme resolves high frequency components of the solution nearly as well as its central counterparts while it has better stability property owing to added dissipation at (only) high wavenumbers. The scheme also has excellent DRP property. Three numerical tests have been carried out with the new scheme. The scheme very efficiently suppresses spurious oscillations as evident from a linear wave propagation problem. Its numerical dispersion property and resolution of peaks is superior to previous upwind schemes, both compact and explicit, as seen from the solution of the two-dimensional scalar transport equation. The scheme is also seen to give accurate results for a linear acoustic problem.

References

[1] C. Canuto, M.Y. Hussaini, A. Quarteroni, T.A. Zang, Spectral Methods in Fluid Dynamics, Springer, New York, 1987.
[2] Z. Kopal, Numerical Analysis, second ed., Wiley, New York, 1961.
[3] S.K. Lele, Compact finite difference schemes with spectral-like resolution, J. Comput. Phys. 103 (1992) 16–42.
[4] R. Vichnevetsky, J.B. Bowles, Fourier Analysis of Numerical Approximations of Hyperbolic Equations, SIAM, Philadelphia, 1982.
[5] R.S. Hirsch, Higher order accurate difference solutions of fluid mechanics problems by a compact differencing technique, J. Comput. Phys. 19 (1975) 90–109.
[6] Y. Adam, Highly accurate compact implicit methods and boundary conditions, J. Comput. Phys. 24 (1977) 10–22.
[7] T. Kawamura, H. Takami, K. Kuwahara, New higher order upwind scheme for incompressible Navier–Stokes equations, Fluid Dynamics Research 1 (1985) 145–162.
[8] X. Zhong, High-order finite-difference schemes for numerical simulation of hypersonic boundary-layer transition, J. Comput. Phys. 144 (1998) 662–709.
[9] T.K. Sengupta, G. Ganeriwal, S. De, Analysis of central and upwind compact schemes, J. Comput. Phys. 192 (2003) 677–694.
[10] Y. Li, Wavenumber-extended high-order upwind-biased finite-difference schemes for convective scalar transport, J. Comput. Phys. 133 (1997) 235–255.
[11] M.M. Rai, P. Moin, Direct simulations of turbulent flow using finite-difference schemes, J. Comput. Phys. 96 (1991) 15–53.
[12] D.W. Zingg, H. Lomax, H. Jurgens, High accuracy finite difference schemes for linear wave propagation, SIAM J. Sci. Comput. 17 (1996) 328–346.
[13] N.A. Adams Shariff, A high-resolution hybrid compact-ENO scheme for shock-turbulence interaction problems, J. Comput. Phys. 127 (1996) 27–51.
[14] Z. Haras, S. Ta'asan, Finite difference schemes for long-time integration, J. Comput. Phys. 114 (1994) 265–279.
[15] P.C. Chu, C. Fan, A three-point sixth-order non-uniform combined compact difference scheme, J. Comput. Phys. 148 (1999) 663–674.
[16] R. Hixon, E. Turkel, Compact implicit maccormack-type schemes with high accuracy, J. Comput. Phys. 158 (2000) 51–70.
[17] J.M.C. Pereira, J.C.F. Pereira, Fourier analysis of several finite difference schemes for the one-dimensional unsteady convection-diffusion equation, Int. J. Numer. Meth. Fluids. 36 (2001) 417–439.
[18] B. Gustafsson, H.-O. Kreiss, A. Sundstrom, Stability theory of difference approximations for mixed initial boundary value problems II, Math. Comput. 26 (1972) 649–686.
[19] M.H. Carpenter, D. Gottlieb, S. Abarbanel, The stability of numerical boundary treatments for compact high-order finite difference schemes, J. Comput. Phys. 108 (1993) 272–295.
[20] C.K.W. Tam, J.C. Webb, Dispersion-relation-preserving finite difference schemes for computational acoustics, J. Comput. Phys. 107 (1993) 262–281.